Advancing 5G Communication Systems: A Novel Method for OOBE Suppression in Filter-OFDM Waveforms

Ammar Ahmed Falih*, Siti Barirah Ahmad Anas, Mohd Fadlee Bin A. Rasid, and Marsyita Binti Hanafi

Department of Computer and Communication Systems Engineering, Faculty of Engineering, Universiti Putra Malaysia, 43400 UPM Serdang, Selangor, Malaysia

Email: ammaralsaedi2006@gmail.com (A.A.F.); barirah@upm.edu.my (S.B.A.A.); fadlee@upm.edu.my (M.F.B.A.R.); marsyita@upm.edu.my (M.B.H.)

*Corresponding author

***Abstract*—Today's 5th Generation (5G) wireless communications systems count heavily on Orthogonal Frequency Division Multiplexing (OFDM) waveforms. Numerous concerns regarding OFDM-based Long-Term Evolution (LTE) communication limitations have not been thoroughly explored. In contrast, Out-of-Band Emissions (OOBE) occur when a signal is transmitted or received outside the accessible frequency range and poses a problem. This situation is a significant obstacle to creating state-of-the-art 5G communication technology. Some thoughts have been given to modifying the OFDM filters for 5G communications due to their resistance to Inter Carrier Interference (ICI) and Inter Symbol Interference (ISI). To reduce spectral leakage into neighbouring sub-bands, OFDM-based waveforms require pulse windowing. This paper proposes a Kaiser-Blackman A (KBA) filter that shows Key Performance Indicators (KPIs) in the simulation concerning OOBE with minimal complexity. The filter was observed in the Power Spectrum Density (PSD) of the Adjacent Channel Leakage Ratio (ACLR) in the time domain, yielding a result of –170 dBm, which was then measured in the frequency domain at –180 dBm. Comparatively, –220 dBm shows an improvement in performance in the hybrid domain, unlike conventional filters' baseline performance. As a result, low latency has been achieved, which is considered a critical challenge of 5G communication and beyond.**

***Keywords*—Orthogonal Frequency Division Multiplexing (OFDM), f-OFDM, Power Spectral Densities (PSD), Bit Error Rate (BER), Peak to Average Power Ratio (PAPR), Out-Of-Band Emission (OOBE) and Adjacent Channel Leakage Ratio (ACLR)**

I. INTRODUCTION

Researchers have examined and used Orthogonal Frequency Division Multiplexing (OFDM) for over a decade in both wired and wireless broadband standards [1]. In addition to being used in the vast majority of wireless standards [2], such as variants of IEEE 802.11 and IEEE 802.16, LTE-advanced, and 5G [3, 4]. OFDM is now a part of the broader class of discrete Multi-Tone Transmission (DMT) standards, such as Asymmetric Digital Subscriber Line (ADSL) and Digital Video Broadcasting Cable (DVB-C). The benefits of orthogonality allow the available bandwidth to be partitioned into a set of small subcarriers that are closely distanced. Adaptive modulation methods can also be used on subcarrier bands to improve the adequate bandwidth. High data rates, resistance to multi-path fading, and simple implementation are only some of the benefits of OFDM [5]. Here, research finds a single formula for the spectral characteristics of OFDM, Filter Bank Multicarrier (FBMC), and F-OFDM signals. It is more than simply a standard representative; it has also garnered increased interest from the business world and the academic community. Conformity with spectrum-regulating masks is obligatory in wireless communication systems [6]. In this sense, spectral behaviour is a crucial indicator of performance. The advantages and disadvantages (such as out-of-band emission) of OFDM, FBMC, and F-OFDM may be systematically compared with the right choice of parameters using this unified spectrum framework (such as the various choices of pulse shaping or spectrum shaping filters, among others). In addition to helping make comparisons, this shared framework might motivate the creation of novel techniques for transmit-receive signal processing in a generic multicarrier system. Finally, quantification is established to estimate the sideband envelopes more efficiently using the unified spectrum expression.

Due to its efficiency, Orthogonal Frequency Division Multiplexing (OFDM) is presently employed in various unique and wireless communication systems. However, OFDM has a high Peak to Average Power Ratio (PAPR) [4] and is susceptible to Inter Carrier Interference (ICI) [3]. In addition, Inter Symbol Interference (ISI) occurs when the channel distribution delay is greater than the length of the Cyclic Prefix (CP) [7]. Researchers have devised innovative strategies for 5G networks to overcome these

Manuscript received July 25, 2024; revised September 9, 2024; accepted October 10, 2024; published March 19, 2025.

limitations. When f-OFDM first emerged, the filtered-OFDM system used a one-filter system for the sharper OOB spectrum characteristics. Still, they later converted to a multiple-filter method, which became pretty comparable to the Universal Filtered Multicarrier (UFMC) [1]. The F-OFDM is currently constructed using the Hanning filter and other optimisation methods. It has been noted that the Hanning filter's leaky spectrum results in out-of-band emissions since the side-lobe fall rate of the filter is flat [8]. It was suggested that the Kaiser filter might replace the standard filter [8], which has a sidelobe fall rate of –24 dB/octave rather than 0 dB/octave. In some cases, using current methods for side-lobe suppression can reduce the spectral efficiency of a system or the BER performance. Previous literature has highlighted some of the issues with these solutions.

Furthermore, state-of-the-art methods do not address the characteristic of increased OOBE in OFDM-based waveforms. High-peak-power signals passing through High-Power Amplifiers (HPA) can re-increase the spectral sidelobes, misguiding the benefits of sidelobe suppression. Massive signal shifts can cause in-band distortions, such as widened modulation sidebands or spectral regrowth in increasingly modulated signals. All radio communication transmitters employing HPAs use sufficient power during transmission to ensure that all recipients receive a strong signal. HIGH-Performance Antennas (HPAs) are typically placed in the saturation zone to maximise performance. However, this placement also introduces out-of-band spectral recurrence [9]. The research to date has focused on OOBE rather than PAPR due to the increase in the OOBE in the 5G waveform led to the non-linearity signals on the RF chain, and the power signal will be toggling. Moreover, enhancing the filter length to lower the OOBE could impact the throughput and latency, particularly when combined with the traditional windowing and filtering method. The fast sidelobe rate drop is another thing that causes significant changes in the signal. This, in turn, causes in-band distortions by the HPAs, which leads to higher PAPR [10]. The Blackman filter's rapid fall in sidelobe rate contributes to the issue of spectral regrowth, indirectly contributing to reducing the OOBE that is considered one challenge in the 5G system. It is crucial to identify solutions to the OOBE problem that do not increase out-of-band emissions [7, 11–13]. This paper focuses on the following:

- Designing a new windowing filter to improve the 5G waveform's spectral efficiency with OOB reduction and without harmful interference.
- The distinct 5G waveform is modelled by fusing F-OFDM with modulator-side windowing or filtering.
- Filtered OFDM are proposed as filter-based definitions of CP-OFDM, respectively, to account for exceptional cases.

In previous works, to meet the higher data rates expected with a new class of services offered by 5G systems, the lower layer of the 5G systems has to be flexible. To do this, 5G waveforms will need to provide many accesses to accommodate the features of the various wired and wireless communication services that are expected in the future. In light of this, the waveforms must be able to accommodate many traffic types simultaneously within the same frequency range. Waveforms of CP-OFDM and the filtered f-OFDM utilised in 4G networks are compared. Additionally, the multicarrier modulation waveform generated by a filter bank is assessed for its potential as a 5G waveform. In addition to accommodating various forms of traffic, future 5G systems would need to utilise spectrum localisation to solve issues arising from spectrum fragmentation. The 5G waveforms' orthogonality and synchronisation will partly meet these needs. Further, while serving many users, adopting 5G waveforms will significantly reduce the amount of signalling information. The new waveforms will support multiple input and output use cases. Reducing OOB transmit power is the primary objective of waveform shaping methods used in orthogonal frequency division multiplexing systems.

Recent efforts to enhance 5G waveforms and lower OOBE are summarised in Ref. [14], along with numerous others that have come before. The broad categories these methods fall into are frequency domain, precoding matrices, and symbol mapping [15]. Adaptive Symbol Transition (AST) [16] is one of the time domain strategies that inserts between two-time blocks to address the OOBE problem. However, it incurs spectrum efficiency losses and has a data-dependent design. Some filters are inserted in the time domain, but many filtering approaches are wasteful in terms of the extension of the symbol, resulting in a decrease in spectrum efficiency [17, 18]. As a filtering method, windowing is another time domain approach that uses a window function [3]. Precoding matrices comprise the second category of methods [19]. Guard Subcarriers (GS) are proposed in Ref. [20], wherein zero-input subcarriers are reserved at channel edges. While it solves the problem, it has lower spectral efficiency. The Carrier Cancellation (CC) technique described in Ref. [12] is similar to that described in Ref. [15], with the exception that its idea is to reserve a subcarrier on the edges with non-zero input, and it also experiences the same spectrum efficiency loss and data-dependent design issues.

The concept of Subcarrier Weighting (SW) is suggested to improve the performance of OFDM and 5G waveforms [16]. It involves assigning different coefficients to each subcarrier. However, this approach has a design issue that depends on the data used. The use of a precoding matrix in Refs. [17, 18] results in a decrease in spectral efficiency since it serves several tasks for different approaches. The techniques for symbol mapping are outlined in Refs. [19–22]. In their study, the authors suggest a Multiple-Choice Sequence (MCS) that utilises multipath streams for selection. However, this approach results in significant overhead, ultimately decreasing spectral efficiency. Nevertheless, the expansion of Constellation [21, 22] can enhance OOBE performance, even if it necessitates more transmit power and a deterioration in Bit Error Rate (BER) [20]. The proposed approach involves using continuous signals and their derivatives to develop an N-Continuous OFDM structure and utilise techniques to reduce OOB interference in the presence of multipath channels. The iteration decoder is the primary constraint in this design since it substantially amplifies the system's overhead.

This paper's organisation follows: Section II reviews the F-OFDM waveform. We recommend studying Section III, which covers the 5G wave windowing method and each contender. Section IV provides a summary of filtering with windowing. In Section V, we discussed why we searched for shape candidate criteria and presented the wave patterns we saw. Section VI proposes a hybrid technique under the new KPI for assessing candidate performance, which is prevalent in 5G waveform research. In Section VII, we introduce the hybrid method. Thus, the search will be discussed, and a hybrid technique will be proposed to minimise the 5G waveform and display the wave patterns in Section VIII. This article finishes with Section IX.

II. F-OFDM Architecture

In addition to CP-OFDM, W-OFDM and Filtered-OFDM (f-OFDM) [23–25] is a micro-filtered multicarrier system with a more versatile filtering resolution. As shown in. Fig. 1, the time-frequency grid is partitioned differently depending on the channel characteristics and use cases. Although more challenging to implement than CP-OFDM, F-adaptability OFDM allows it to use a broader range of numerologies (including bandwidth, sub-carrier spacing, CP duration, and transmission time interval) [26–28]. Considering all B blocks, the baseband F-OFDM signal is displayed as Eq. (1) [26].

$$S[t] = \sum_{b=0}^{B-1}\sum_{m=0}^{M-1}\sum_{l=0}^{L_b-1}\sum_{n=0}^{N-1} d_{m,n}^{b} g_b[l] e^{j2\pi k(n-t-mL_{CP})/N} \quad (1)$$

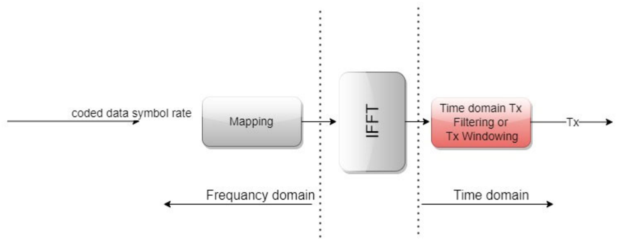

Fig. 1. F-OFDM block diagram in the time domain.

The notation denotes the complex data transmitted across the block, nth subcarrier, and m^{th} sub-symbol. Meanwhile, it represents the windowing function in the frequency domain of a time domain Finite Impulse Response (FIR) filter applied to both blocks. Lastly, it refers to the size of the cyclic prefix. In contrast to UFMC, F-OFDM retains the Cyclic Prefix (CP), as demonstrated by Eq. (1). Consequently, this necessitates a receiver that is less complex and more resilient to Inter-Symbol Interference (ISI). The rectangular shape is considered an optimal choice for the window function in the frequency domain, denoted as L_b-by-b. However, mapping this particular entity results in a synchronised form of unlimited length in the time domain, making it inappropriate for the intended purpose. To perform this filtering, windowed synchronise routines must be used. Further details regarding different types of filters can be found in Ref. [29]. Fig. 1 is a block diagram representation of the significant components of a conventional f-OFDM transmitter. In contrast to other sub-band-wise filtering algorithms, such as UFMC, F-OFDM distinguishes itself by employing matched filtering and utilising receiver IFFT/FFT blocks of comparable sizes. The F-OFDM waveform has many of the same benefits as other frequency-localised waveforms. It has low Out-Of-Band Emission (OOBE), can support asynchronous transmission, works with various numerologies, and doesn't need as many guards' tones. Using shorter filter lengths in F-OFDM results in the inability to achieve low OOBE levels, a characteristic that subcarrier-wise filtered multicarrier systems possess. Nevertheless, it can support the Multi-Input Multi-Output (MIMO) transmission methodology without requiring Sequential Interference Cancellation (SIC) methods. Although F-OFDM offers numerous advantages compared to CP-OFDM, its complexity remains a notable limitation.

III. Reducing the OOBE in F-OFDM

The transmission synthesis includes the amalgamation of distinct sub-band signals, as seen in Fig. 1. During the uplink (UL) transmission, users only use the frequency band given to them. In contrast, during the downlink (DL) transmission, data is disseminated to various consumers using separate sub-modules throughout all accessible frequency bands. The graphic depicts the sequential steps involved in constructing a signal composed of a single sub-band. The time domain representation of the Ni complex QAM symbol is generated using the Inverse Discrete Fourier Transform (IDFT) technique. Furthermore, additional sub-band filtering is performed. Eq. (2) [30] represents the summation of sub-band-wise filtered components, which form the transmit vector in the time domain for a specific multicarrier signal.

$$S(t) = \sum_{i=1}^{B} F_i V_i S_i \quad (2)$$

where is a matrix of size N, represents the columns of the IFFT matrix that are most important in terms of sub-band location, and is a Toeplitz matrix of size (N+N_filter-1) time N that contains the Finite Impulse Response (FIR) that makes the convolution possible. Eqs. (3−5) define the rewritten signal without the addition:

$$\underline{F} = [F_1 F_2 F_3 \ldots F_B] \quad (3)$$

$$\underline{V} = diag\ [V_1 V_2 V_3 \ldots V_B] \quad (4)$$

$$\underline{S} = [S_1^T S_2^T S_3^T \ldots S_B^T]^T \quad (5)$$

By shrewdly stacking filter matrices, an IDFT matrix is created, and all the data symbols are merged into a single column. Thus, the value of $S(t)$ is equal to FVS.

$$S(t)=FVS \quad (6)$$

Table I presents the essential design parameters. In this particular scenario, the Sub-module associated with an F-OFDM transmitter controls the broadcast frequency selection for a B entity. To implement the methodology on a segmented spectrum, it is necessary to consider the quantity of feasible spectral sub-bands (B). Comparable to Long Term Evolution (LTE) [31]. Nevertheless, it is possible to partition the single sub-band into smaller segments of uniform size within each sub-band. These segments, known as Physical Resource Blocks (PRB), constitute the spectral components. When selecting a filter, two crucial factors are the ability to modify the filter's main lobe and side lobe attenuation and the window's width. The values of the parameters utilised in our analysis will be shown in the section dedicated to the simulated findings.

TABLE I. CONFIGURATION SETTINGS

Parameters	Meaning
B	Sub-bands of Total Number
Ni (blockSize)	Subcarriers in sub-band *i*
N	Overall Subcarriers
Filter Length	Tap the length of the filter.

IV. WINDOWING MODELS

OFDM windowing is based on partitioning the available transmission bandwidth into a series of orthogonal subcarriers. Following established conventions, an Orthogonal Frequency Division Multiplexing (OFDM) signal can be mathematically expressed using Eq. (7) in the following:

$$S(t) = \sum_{n=-\infty}^{\infty} S_n(t - nT) \quad (7)$$

Consequently, many pieces are integrated to construct the conventional architecture of an OFDM transmitter. The sequential sequence of data symbols will undergo a conversion process, commonly called symbol mapping, resulting in a parallel sequence. The Inverse Fast Fourier Transform (IFFT) block will transmit all the modulated data symbols on OFDM carriers. Subsequently, the parallel stream will be serialised and transformed to a frequency appropriate for transmission. Various iterations of traditional Orthogonal Frequency Division Multiplexing (OFDM) have been developed. To mitigate Inter-Symbol Interference (ISI), time guard intervals, such as Cyclic Prefix (CP) or Zero Padding (ZP), can be inserted between consecutive Orthogonal Frequency-Division Multiplexing (OFDM) symbols [32]. Windowed Orthogonal Frequency Division Multiplexing (WOFDM), alternatively referred to as OFDM with Weighted Overlap (WOLA) [33], retains the fundamental framework of OFDM systems while mitigating computational complexity and facilitating the incorporation of Multiple-Input Multiple-Output (MIMO) techniques. Therefore, the mitigation of OOBE in OFDM [34] is accomplished by substituting the abrupt edges of the rectangular pulse with a more gradual windowing function at the transmitting end and by overlapping adjacent Windowed Overlap-Add (WOLA) symbols. This study will primarily enhance classic OFDM filtering to the extent that generalisation is feasible.

V. TIME DOMAIN MODEL AND NEW FILTER

Filtered-Orthogonal Frequency Division Multiplexing (F-OFDM) is a spectrum-shaping approach that utilises filtering. The primary differentiation is in the design of the band-pass filter. The prototype filter is a rectangular pulse that spans the Orthogonal Frequency Division Multiplexing (OFDM) symbol and the Cyclic Prefix (CP). The 3rd Generation Partnership Project (3GPP) standard mandates the utilisation of Filtered Orthogonal Frequency Division Multiplexing (F-OFDM) in the 5th Generation (5G) waveform, with the specific requirement of employing Hanning filtering to mitigate OOBE. The Tx filter has been carefully engineered to effectively minimise OOBE interference [35]. To minimise the OOBE, the Hanning filter is employed, whereby the length of the Transmit (Tx) filter is configured to be half the length of the Filtered Orthogonal Frequency-Division Multiplexing (F-OFDM) symbol. The calculation of the TX filter involves the multiplication of an ideal bandpass filter and a time domain mask. Consequently, creating or picking the filters dynamically is imperative, considering the tone allocation. The filter's OOB suppression and ISI effect are subject to variation based on the tone allocation, given that the total filter length remains constant. Another concern of utilising F-OFDM in low-latency scenarios is the extended group delay resulting from implementing lengthy filters. The concatenated transmit and receive filter in Ref. [36] necessitates a processing delay of one Orthogonal Frequency Division Multiplexing (OFDM) symbol. The utilisation of Hanning windowing can substantially increase switching overhead inside the Time Division Duplexing (TDD) spectrum due to the considerable processing delay involved.

The generation of the F-OFDM waveform may be similar to the "time domain windowing technique", which is also used in creating the WOLA waveform. The provided example [37] illustrates the previously indicated equivalence. The synthesis of F-OFDM waveforms may be efficiently performed using various windowing methods [38]. Systems lacking Multiple-Input Multiple-Output (MIMO) capability often exhibit more complex modulation and demodulation processes in Frequency Division Multiplexing (F-OFDM) compared to other Cyclic Prefix-Orthogonal Frequency Division Multiplexing (CP-OFDM) waveforms. The increased complexity may be partially attributed to using just half the Inverse Fast Fourier Transform (IFFT) length when using standard windowing approaches. The Hanning windowing function, as specified by the 3GPP standard [39], was used for the wiring in Eq. (8) of the F-OFDM system.

$$\omega(k)_{Hann} = 0.5 - 0.5 \times cos\,(2 \times Pi \times k/N - 1) \quad (8)$$

Numerous researchers have employed the Kaiser filter, precisely the variant [40, 41], to mitigate the limitations associated with the conventional methodology. The utilisation of Finite Impulse Response (FIR) coefficients in the Kaiser filter window [42] is contingent upon the parameterisation of such coefficients, which is determined by the level of attenuation exhibited by the side lobes. The

Blackman window is considered optimal because of its ability to effectively reduce the extent of the primary lobe while simultaneously optimising the suppression of the secondary lobes. Fig. 2, which examines the 5G filters used in F-OFDM, indicates that the Blackman filter is the best choice for developing and building a new tuning filter. This filter is essential for enhancing the directional characteristics of a radio antenna [43–46].

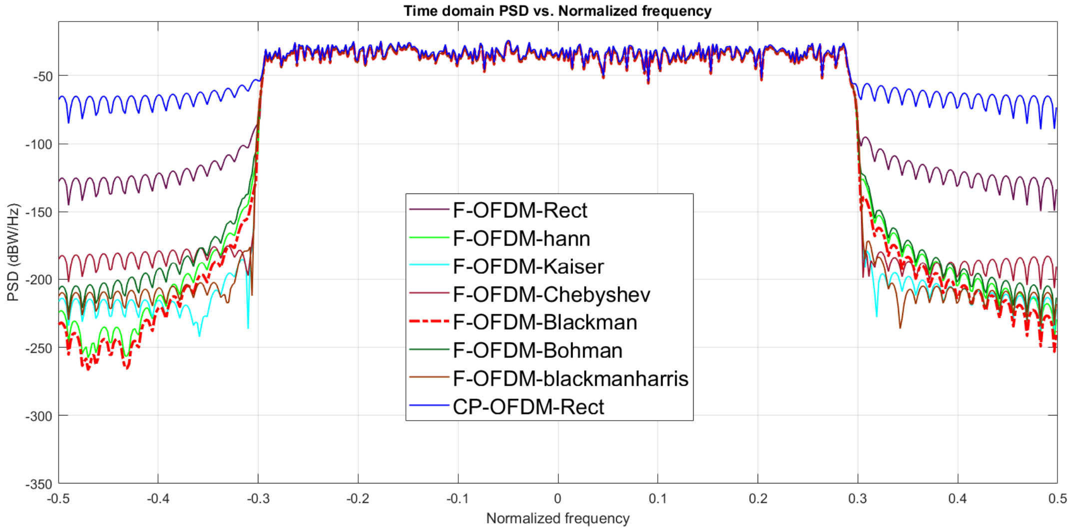

Fig. 2. PSD in F-OFDM with different 5G filters in the time domain.

The evaluation of a novel filter will be undertaken, specifically focusing on the Kaiser and Blackman filters as depicted in Eq. (9). The Kaiser Windowing function ω(k) is defined by Eq. (10) [47] for an N-point sample where beta is the windowing parameter. To generate and further develop the novel KBA filter, the expiration of the filter is illustrated as follows:

$$\omega_{KBA}(k) = \omega_{modified\ Kaiser}(k) \times \omega_{Blackman}(k) \qquad (9)$$

$$w_{kaiser}(k) = \frac{I_0(\text{ƀ})}{I_0(\text{Ч})} \qquad (10)$$

$$= \frac{I_0\left(\beta\sqrt{1-\left(\frac{k}{N/2}\right)^2}\right)}{I_0(\beta)} \qquad (11)$$

$$\mathrm{I}_0(\text{ƀ}) = \mathrm{I}_0\left(\beta\sqrt{1-\left(\frac{k}{\frac{N}{2}}\right)^2}\right) \qquad (12)$$

$$I_0(\text{ƀ}) = N \times \frac{\sin\left(\sqrt{\left(\frac{Nk}{2}\right)^2-\beta^2}\right)}{\sqrt{\left(\frac{Nk}{2}\right)^2-\beta^2}} \qquad (13)$$

$$I_0(\text{Ч}) = I_0(\beta) \qquad (14)$$

$$I_n(x) = -(i)^n \times j_n(ix) \qquad (15)$$

$$j_n(x) = \frac{\sqrt{2}}{\sqrt{x\pi}} \times \cos\cos\left(x - \frac{(2n+1)\times\pi}{4}\right) \qquad (16)$$

Eq. (16) in Eq. (15):

$$I_n(x) = -(i)^n \times \frac{\sqrt{2}}{\sqrt{ix\pi}} \times \cos\cos\left(ix - \frac{(2n+1)*\pi}{4}\right) \qquad (17)$$

According to the 1st order from the Bessel equation, n=0 as we are using with x= beta:

$$I_0(\beta) = -(i)^0 \times \frac{\sqrt{2}}{\sqrt{i\beta\pi}} \times \cos\left(i\beta - \frac{(2\times 0+1)\times\pi}{4}\right) \qquad (18)$$

$$I_0(\beta) = -\frac{\sqrt{2}}{\sqrt{i\beta\pi}} \times \cos\left(i\beta - \frac{\pi}{4}\right) \qquad (19)$$

Eq. (13) and Eq. (19) in Eq. (10):

$$w_{modified\ kaiser}(k) = \frac{N*\frac{\sin\left(\sqrt{\left(\frac{Nk}{2}\right)^2-\beta^2}\right)}{\sqrt{\left(\frac{Nk}{2}\right)^2-\beta^2}}}{-\frac{\sqrt{2}}{\sqrt{i\beta\pi}}*\cos\left(i\beta-\frac{\pi}{4}\right)} \qquad (20)$$

$$w_{modified\ kaiser}(k) = -\frac{N\times\sqrt{i\beta\pi}}{\sqrt{2}\times\sqrt{\left(\frac{NK}{2}\right)^2-\beta^2}} \times \frac{\sin\left(\sqrt{\left(\frac{Nk}{2}\right)^2-\beta^2}\right)}{\cos\left(i\beta-\frac{\pi}{4}\right)} \qquad (21)$$

$$w_{modified\ kaiser}(k) = -\frac{N\times\sqrt{i\beta\pi}}{\sqrt{2}*\sqrt{\left(\frac{Nk}{2}\right)^2-\beta^2}} \times \sec\left(i\beta - \frac{\pi}{4}\right) \times \sin\left(\sqrt{\left(\frac{Nk}{2}\right)^2-\beta^2}\right) \qquad (22)$$

When alpha is equal to 3, a specific part of the equation will only involve beta (Ȼ). Based on the beta test, we have determined that the most appropriate and least complex solution occurs when a beta is less than or equal to 3. Therefore, this solution will be applied to the corresponding portion of Eq. (22) as shown below:

$$\text{Ȼ} = \frac{\sqrt{i3\pi}}{2} \times \sec\left(i3 - \frac{\pi}{4}\right) = 0.7772 - 0.211i \qquad (23)$$

Eq. (23) in Eq. (22):

$$w_{kaiser}(k) = -\frac{N*(0.7772-0.211i)}{\sqrt{\left(\frac{Nk}{2}\right)^2-\alpha\pi}} \times \sin\left(\sqrt{\left(\frac{Nk}{2}\right)^2-\alpha\pi}\right) \qquad (24)$$

We will neglect the imaginary at the Eq. (25), so:

$$w_{modified\ kaiser}(k) = -\frac{N\times 0.78}{\sqrt{\left(\frac{Nk}{2}\right)^2-\alpha\pi}} \times sin\ sin\ \left(\sqrt{\left(\frac{Nk}{2}\right)^2-\alpha\pi}\right) \quad (25)$$

$$\omega_{blackman}(k) = 0.42 - 0.08\ cos\left(\frac{2\pi k}{N-1}\right) + 0.5\ cos\left(\frac{4\pi k}{N-1}\right) \quad (26)$$

Eq. (25) and Eq. (26) in Eq. (9):

$$w_{KBA}(k) = -\frac{N\times 0.78}{\sqrt{\left(\frac{Nk}{2}\right)^2-\alpha\pi}} \times sin\left(\sqrt{\left(\frac{Nk}{2}\right)^2-\alpha\pi}\right) \times (0.42 - 0.08\ cos\left(\frac{2\pi k}{N-1}\right) + 0.5\ cos\left(\frac{4\pi k}{N-1}\right)) \quad (27)$$

$$w_{KBA}(k) = -\frac{N\times 0.78}{\sqrt{\left(\frac{Nk}{2}\right)^2-\alpha\pi}} \times sin\left(\sqrt{\left(\frac{Nk}{2}\right)^2-\alpha\pi}\right) \times \left(0.42 - 0.08\ cos\left(\frac{\pi k}{N-1}\right)^2 + 0.5\ cos\left(\frac{\pi k}{N-1}\right)^4\right) \quad (28)$$

$$Д_k = \sqrt{\left(\frac{Nk}{2}\right)^2-\alpha\pi} \quad (29)$$

$$\rho_k = \frac{\pi k}{N-1} \quad (30)$$

$$w_{KBA}(k) = -\frac{N\times 0.78}{Д_k} \times sin\ (Д_k) \times (0.42 - 0.08\ cos\ (\rho_k)^2 + 0.5\ cos\ (\rho_k)^4\ ) \quad (31)$$

$$w_{KBA}(k) = \frac{-N\times 0.78 sinsin\ (Д_{Nk})\times(0.42-0.08\ coscos\ (\rho_{Nk})^2 + 0.5coscos\ (\rho_{Nk})^4\ )}{Д_{Nk}} \quad (32)$$

$$w_{KBA}(k) = \frac{Nsinsin\ (Д_{Nk})(0.062cos\ (\rho_{Nk})^2 - 0.39cos\ (\rho_{Nk})^4 - 0.327\ )}{Д_{Nk}} \quad (33)$$

VI. FIR Filter Design Using Windowing Technique

The frequency response of a wanted filter exhibits periodicity and can be represented by an expansion in terms of a Fourier series. The series that emerges as a result is expressed as [48]:

$$H_d(e^{jw}) = \sum_{n=-\infty}^{\infty} h_d(n)e^{-jwn} \quad (34)$$

where:

$$H_d(e^{jw}) = \frac{1}{2\pi}\int_{-\pi}^{\pi} H_d(e^{jw})e^{-jwn}dw \quad (35)$$

The concept referred to as Fourier coefficients is characterised by having a finite length.

One potential method for acquiring a Finite Impulse Response (FIR) filter involves truncating the finite series by setting the value of n to be approximately equal to ∓[(*N*-1)/2], where N represents the length of the desired sequences.

However, when the Fourier series is abruptly truncated, oscillations occur in both the pass and stop bands. The observed oscillations can be attributed to the gradual convergence of the Fourier series, a process commonly referred to as the Gibbs phenomenon.

To mitigate the occurrence of these oscillations, the filter's Fourier series coefficients undergo modification through the multiplication of the infinite impulse response by a finite weighing sequence denoted as w(n), commonly referred to as a windowed sequence [44].

$$w(n) = w(-n) = \left[\neq 0\ \ |n| \leq \left|\frac{N-1}{2}\right| = 0\ \ |n| > \left|\frac{N-1}{2}\right|\ \right] \quad (36)$$

By doing the multiplication of the window sequence $w(n)$ with $h_d(n)$, a finite duration sequence $h(n)$ It is obtained to fulfil the desired magnitude response.

$$h(n) = \left\{h_d(n).w(n)\ \ \ |n| \leq \left|\frac{N-1}{2}\right|\ \ 0\ \ \ otherwise\right\} \quad (37)$$

The z transform of the sequence is given by:

$$H(z) = \sum_{n=-\infty}^{\infty} h(n).z^{-n} \quad (38)$$

Then:

$$H(z) = \sum_{n=-\frac{N-1}{2}}^{\frac{N-1}{2}} h(n).z^{-n} \quad (39)$$

$$= h\left[-\frac{N-1}{2}\right].z^{\frac{N-1}{2}} + \cdots + h(-z).z^2 + h(-1).z^1 + h(0) + h(1).z^{-1} + h(2).z^{-2} + \cdots + h\left(\frac{N-1}{2}\right).z^{-\frac{N-1}{2}} \quad (40)$$

$$H(z) = h(0) + \sum_{n=1}^{\frac{N-1}{2}}[h(n).z^{-n}h(-n).z^n] \quad (41)$$

The impulse response, denoted as *h*(*n*), exhibits symmetry at n=0, meaning that it satisfies the condition *h*(*n*) = *h*(−*n*). The fourth equation can be expressed as:

$$H(z) = h(0) + \sum_{n=1}^{\frac{N-1}{2}} h(n).[z^{-n} + z^n] \quad (42)$$

The transfer function mentioned above is deemed non-physically realisable [49, 50].

The concept of realizability can be achieved by multiplying Eq. (5) with the factor of $z^{-\frac{N-1}{2}}$.

$$H'(z) = H(z), z^{-\frac{N-1}{2}} \quad (43)$$

$$= z^{-\frac{N-1}{2}}\left[h(0) + \sum_{n=1}^{\frac{N-1}{2}} h(n).[z^{-n} + z^n]\right] \quad (44)$$

VII. Desired Characteristics of Windowing Function

The primary objective of windowing is to concentrate most of the energy inside the central lobe of the frequency response while simultaneously ensuring that this lobe is relatively tiny.

It is desirable for the maximum sidelobe level of the frequency response to exhibit a diminutive magnitude.

The energy of the side lobes in the frequency response should exhibit a quick reduction as the angular frequency approaches π.

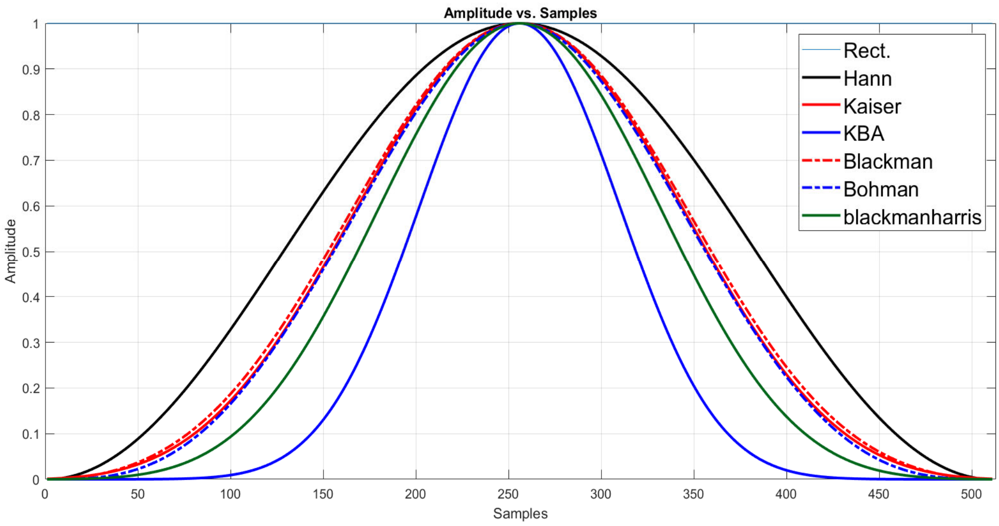

Fig. 3. The time-domain characteristics for the new filter (window) KBA.

The Discrete Fourier Transform (DFT) uses the compounding window in this context to produce W(n) samples. These samples are then normalised so that their maximum amplitude equals one. The parameter represents the computational process identifying the level difference between the primary and secondary lobes. In this context, a score of 3.0 signifies that the side lobes exhibit a reduction in sound level of 60.0 dB compared to the main lobe, equivalent to a decrease of 3.0 decades. The length of the sidelobes is used to represent their attenuation. The parameter facilitates the customisation of the Blackman filter window by modifying the algorithmic equilibrium between the primary lobe and the secondary lobes. The time-domain characteristics in Fig. 3 illustrate the optimal parameters, including the length of the Blackman window and the side-lobe attenuation of 60 dB.

A. Mathematical Model in Time Domain

The mathematical representation of F-OFDM in the time domain is expressed as follows:

Input data = d_0, d_1, d_2, …., d_n,

Modulation scheme = 64QAM = A,

$$A = [a_{00}\ a_{1,0}\ \ a_{2,0}\ a_{3,0}\ \ \cdots\ a_{63,0}]$$

Multiply by subcarrier $e^{-j\frac{2\pi kn}{1024}}$.

For 1st carrier = $e^{-j\frac{2\pi n}{1024}}$, where k= 1 and N=1024.

$$(k) = \begin{bmatrix} a_{0,0}e^{-j\frac{2\pi n}{1024}}, a_{1,0}e^{-j\frac{2\pi n}{1024}},\ \ a_{2,0}e^{-j\frac{2\pi n}{1024}}, a_{3,0}e^{-j\frac{2\pi n}{1024}},\ \ \cdots \\ a_{63,0}e^{-j\frac{2\pi n}{1024}}, \end{bmatrix} \tag{45}$$

$x(n) = \ IFFT\ X(k) =$

$$\begin{bmatrix} \frac{X(K)_{00}}{\sqrt{1024}} e^{-j\frac{2\pi n}{1024}} & \cdots & \cdots & \cdots & 0 \\ 0 & \cdots & \cdots & \cdots & 0 \\ \vdots & \vdots & \ddots & \vdots & \vdots \\ 0 & \cdots & \cdots & \cdots & \frac{X(K)_{63,1022}}{\sqrt{1024}} e^{-j\frac{2047\pi n}{1024}} \\ 0 & \cdots & \cdots & \cdots & \frac{X(K)_{63,1023}}{\sqrt{1024}} e^{-j\frac{2048\pi n}{1024}} \end{bmatrix} \tag{46}$$

$$windowed\ Coofitient\ h(n)$$
$$h(n) = [h_0\ h_2\ h_3\ \ \ h_4\ \cdots\ h_{511}\ ] \tag{47}$$

windowing:

$$s(n) = h(n) \times x(n) = \ [y(n)]$$

VIII. Hybrid Domain Model

The hybridisation of the time domain and frequency domain, as depicted in Fig. 4, successfully produces a significant reduction in OOBE and boosts the KPIs for the 5G waveform. Furthermore, the computing complexity remains unchanged while employing the Cyclic Prefix (CP) with filtering OFDM in light of the CP's length, which mitigates both OOBE and Inter-Carrier Interference (ICI) concurrently. This hybrid approach minimises OOBE in the 5G waveform and beyond.

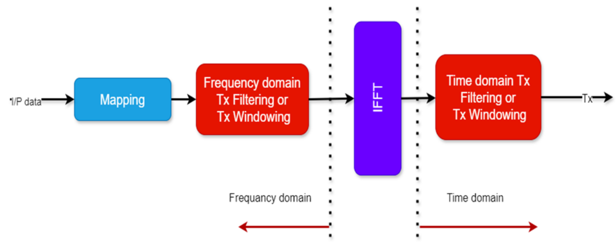

Fig. 4. F-OFDM block diagram in hybrid domain.

A. Mathematical Model in Hybrid Domain

Input data = $d_0, d_1, d_3, \ldots, d_n,$

Modulation scheme = 64QAM = A

$$A = \begin{bmatrix} a_{00}\, a_{1,0} & a_{2,0}\, a_{3,0} & \cdots\ a_{63,0} \end{bmatrix} \quad (48)$$

Windowed matrix (H(K)):

$$H(0) = \begin{bmatrix} H_{0,0}\, H_{0,1} & H_{0,2}\, H_{0,3} & \cdots\ H_{0,511} \end{bmatrix} \quad (49)$$

To have windowing for the A(K) in the frequency domain, we should convolute the A(K) with the windowed coefficient:

$$\mathrm{C}(K) = A(K) \times H(K) \quad (50)$$

So, the windowed matrix will be:

$$H(K) = \begin{bmatrix} H_0 & \cdots & H_{250} & \cdots & H_{511} \\ H_{509} & \cdots & \cdots & \cdots & H_{510} \\ \vdots & \vdots & \ddots & \vdots & \vdots \\ H_{447} & \cdots & \cdots & \cdots & H_{458} \\ H_{448} & \cdots & \cdots & \cdots & H_{457} \end{bmatrix} \quad (51)$$

Windowed in the Frequency domain:

$$C(K) = A(k) \times H(K) = [A(K)] \times [H(K)\,] \quad (52)$$

Multiply by subcarrier $e^{-j\frac{2\pi kn}{1024}}$.

For 1st carrier = $e^{-j\frac{2\pi n}{1024}}$, where k= 1 and N=1024.

$$X(k) = \begin{bmatrix} H_0 a_{0,0} e^{-j\frac{2\pi nk}{1024}}\, H_{511} a_{1,0} e^{-j\frac{2\pi nk}{1024}}\ \ H_{510} a_{2,0} e^{-j\frac{2\pi nk}{1024}}\, H_{509} a_{3,0} e^{-j\frac{2\pi nk}{1024}} \\ \cdots\ H_{448} a_{63,0} e^{-j\frac{2\pi nk}{1024}} \end{bmatrix} \quad (53)$$

$$x(n) = IFFT\ X(k) = [IFFT\ X(K)\,] \quad (54)$$

$$s(n) = [h(n)] \cdot [x(n)\,] \quad (55)$$

IX. Outcomes and Benchmarks

The present study commences by examining the F-OFDM 5G waveform with the MATLAB program used to assess the efficacy of KBA. Unlike F-OFDM, the present study shows an improved ability to accurately locate frequency domain frequencies and better withstand temporal frequency offset changes than CP-OFDM. Furthermore, it is worth noting that low-latency applications benefit more from using shorter filter lengths rather than sub-carrier-wise filtering. However, filters with shorter lengths have restricted powers to block out-of-band emissions. Subsequently, a simulation was performed to assess the performance of F-OFDM using the Kaiser window. The simulation used the same parameters as those used for the Blackman window F-OFDM and the Kaiser F-OFDM. The system was thoroughly assessed using essential KPIs such as PSD, BER, ACLR, and complexity.

The combined Blackman filters and Kaiser windows were combined with the simulated software. Table II presents the key input parameters employed in the simulation. According to the ref. [51], there exists a linear relationship between the Peak-to-Bottom Gain Ratio (PBGR) of a filter inside a single subband and two factors: the length of the filter and the ratio of the number of sub-carriers to the number of sub-bands. This study Posits that Bit Generation Error (PBGR) probability is negligible, as the absence of frequency selectivity among sub-carriers would have no effect. The F-OFDM- FFT 1024 system is characterised by a fractional expression denoting the total number of sub-carriers, equivalent to the filter's length.

TABLE II. Simulation Parameters

Simulation Parameters	CP-OFDM	F-OFDM	Proposed F-OFDM
No. of FFT points	1024	1024	1024
No. of subcarriers in each subband	1024	1024	1024
No. of Physical Resource Blocks (PRB)	14	14	14
No. of subcarriers per resource block	12	12	12
No. of bits in each subcarrier	6	6	6
Filter Length	513	513	513
Cyclic prefix length	72	72	72
Type of filter	Rectangular	Hanning	Kaiser-Blackman
SNR	20	20	20
Sidelobe attenuation factor, dB	45	40	40
Modulation	64QAM	64QAM	64QAM
Tone offset or excess bandwidth	5	4	4
Bata	0	0	3

Several performance metrics are employed to assess the efficacy of the presented methodologies, including PSD, BRE, Signal-to-Noise Ratio (SNR), Peak-to-Average Power Ratio (PAPR), and computational complexity at the transmitter side. Field testing is conducted to examine the effectiveness of the proposed methodologies and the performance of waveforms based on KPIs. In addition, the suggested methods were evaluated compared to existing windowing methods found in the academic literature. This evaluation focused on the performance of reducing OOBE as well as the level of computing complexity.

X. Comparison of the Filters for F-OFDM Waveform

Fig. 1 displays time-domain simulations of CP-OFDM and F-OFDM using the Kaiser filter, the Blackman filter, and a rectangular filter for OFDM. The impulse responses of the filter demonstrate that the pass band of the F-OFDM filter is smaller in contrast to that of the OFDM filter. This discovery indicates that the F-OFDM technique has improved spectral efficiency, particularly when the spectra are fragmented. Fig. 5 illustrates the frequency-domain filter characteristics of both the Blackman and KBA filters. The KBA filter has a roll-off rate of 6 dB per octave, whereas the Blackman filter has a roll-off rate of 0 dB per octave.

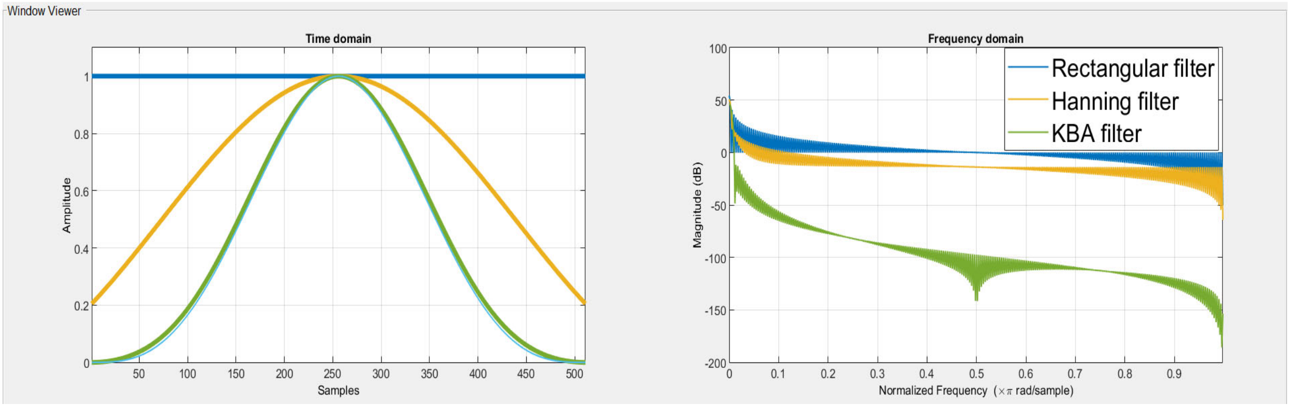

Fig. 5. Specification of the filters.

A. Power Spectral Density Analysis

This study examines the power Spectral Densities Rectangle (PSDR) for F-OFDM with Hanning, Kaiser, and KBA filters and OFDM systems with Additive White Gaussian Noise (AWGN). The receiver is estimated through simulations using the Minimal Squared Error (MSE) approach, with the system running under Additive White Gaussian Noise (AWGN) circumstances at a Signal-to-Noise Ratio (SNR) of 20 dB. The KBA-based F-OFDM has a lower spectral leakage level than the Blackman filter. The examination of the ACLR confirms the results. The measured characteristics are the ACLR, leading, and adjacent channel power. On one side, the PSD frequency (dBW/Hz) for each window function with normalised frequency in the time domain is depicted below Fig. 6. The results of the simulation demonstrated that F-OFDM with KBA yielded the most favourable outcomes in the study of the time domain, specifically in terms of the PSD under conditions of Additive White Gaussian Noise (AWGN) with a Signal-to-Noise Ratio (SNR) of 20 dB and an ACLR of −170.39 dB. In contrast, the Kaiser and Hanning windows yielded comparable outcomes, specifically an ACLR of 85.79 and −80, respectively.

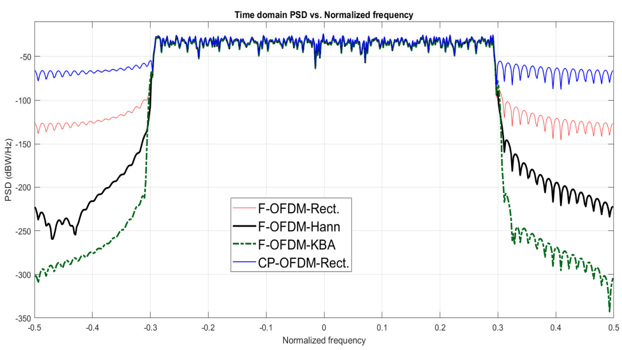

Fig. 6. Time domain analysis for PSD of AWGN SNR = 20 dB in Hanning, KBA, and Rectangular OFDM.

On the other hand, Fig. 7 presents the simulation outcomes for Power Spectral Densities (PSD) compared to normalised frequencies of F-OFDM windows in the frequency domain. The provided figure demonstrates that the F-OFDM KBA, as proposed, yielded superior results (−180.39) in terms of ACLR in the frequency domain compared to alternative OFDM-Kaiser and OFDM-Hanning filters. Notably, the OFDM-Kaiser filter had exceptional results in ACLR, with a value of −99.79, compared to the OFDM-Hanning filter, which produced an ACLR of −80.

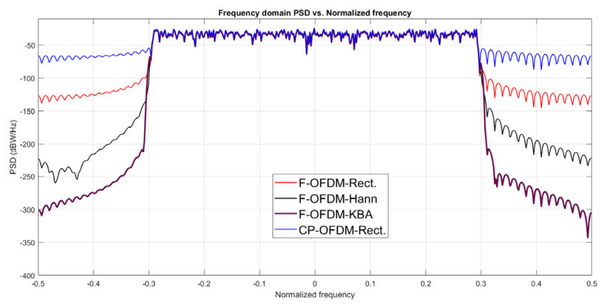

Fig. 7. Frequency domain analysis for PSD of AWGN SNR = 20 dB in Hanning, KBA, and Rectangular OFDM.

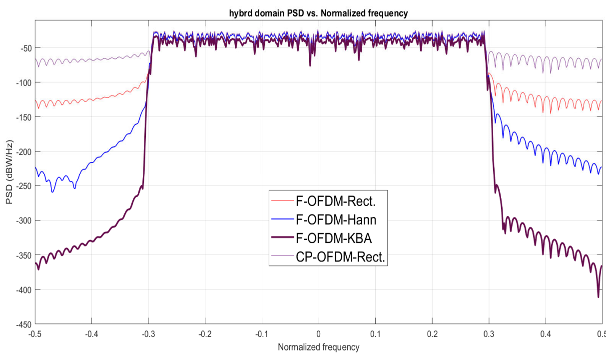

Fig. 8. Hybrid frequency domain analysis of the PSD of AWGN SNR = 20 dB in kaiser, KBA, and rectangular OFDM.

In addition, the PSD study results for the hybrid frequency domain demonstrated favourable outcomes, as depicted in Fig. 8. Moreover, the suggested KBA filter exhibited a significantly higher ACLR of −220.39 compared to the OFDM Kaiser and Hanning filters.

Furthermore, the preceding two observations exhibited remarkably similar results of Anterior Cruciate Ligament Reconstruction (ACLR), with values ranging from –80 to –87.79, respectively.

B. Bit Error Rate (BER)

This section intends to present the simulation results on the BER performance of the KBA-F-OFDM signal using 64-QAM modulation. The data presented in Figs. 9–11 suggest that despite its higher power consumption, the conventional Cyclic Prefix Orthogonal Frequency Division Multiplexing (CP-OFDM) has a comparatively inferior BER performance compared to the F-OFDM, Kaiser, and KBA F-OFDM signals. When the value of B equals 3, Kaiser's BER experienced a slight increase. The observed outcome can be attributed to the absence of shielding between CP-OFDM sub-bands, leading to reciprocal interference. Nevertheless, the simulation outcomes of the BER concerning the Signal-to-Noise Ratio (SNR) of the filters as mentioned above in the temporal domain indicated that the Kaiser-Blackman A (KBA) exhibited superior performance when compared to the OFDM-Kaiser and Hanning filters, as visually depicted in Fig. 9. The simulation results demonstrate that the KBA yields similar outcomes to other windows of OFDM-Hanning and CP-OFDM-Rec, as shown in Figs. 9–11, respectively.

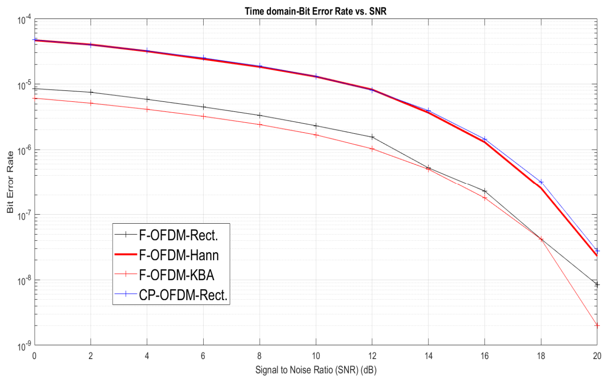

Fig. 9. Time domain evaluation of BER performance for the conventional 64QAM CP-OFDM with the 64QAM F-OFDM-based rectangular, Hanning, and KBA windows.

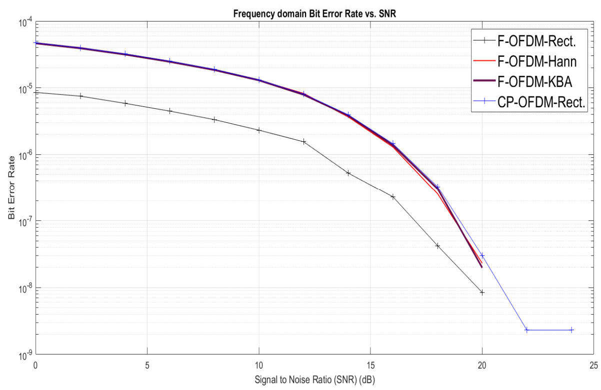

Fig. 10. Frequency domain evaluation of BER performance for the conventional 64QAM CP-OFDM with the 64QAM F-OFDM-based rectangular, Kaiser, and KBA windows.

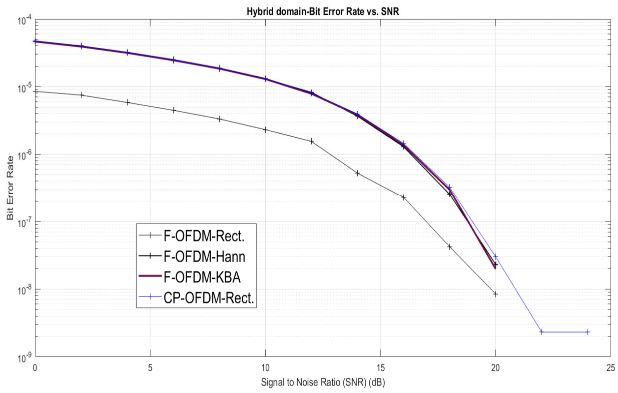

Fig. 11. Hybrid domain evaluation of BER performance for the conventional 64QAM CP-OFDM with the 64QAM F-OFDM-based rectangular, Kaiser, and KBA windows.

C. Pek Average to Power Ratio (PAPR)

This subsection provides an overview of the outcomes obtained from the Peak-to-Average Power Ratio (PAPR) performance simulation for the F-OFDM signal utilising a 64-QAM modulation scheme. The comparative analysis of the Peak-to-Average Power Ratio (PAPR) performance between conventional Cyclic Prefix Orthogonal Frequency Division Multiplexing (CP-OFDM) and Frequency-Offset Orthogonal Frequency Division Multiplexing with Hanning Window (F-OFDM-Hanning) and F-OFDM-KBA signals reveals that the latter two exhibit superior PAPR performance, despite their greater power consumption. This observation is supported by the data presented in Figs. 8–10. The lack of protection between CP-OFDM sub-bands is the cause of this phenomenon. The simulation results in the time domain demonstrated that the KBA outperformed the OFDM-Hanning filter in terms of performance. Additionally, the KBA exhibited similar results to other windows of OFDM-Hanning and CP-OFDM-Rec for Figs. 12–14. The Cross-Correlation Distortion Factor (CCDF) for the F-OFDM-KBA exhibits a value of 0.01 in the temporal domain, which is comparatively higher than its counterparts in the frequency domain (0.001) and the hybrid domain (0.006). Furthermore, the hybrid domain demonstrates a lower minimum power of 3 dB, in contrast to the temporal domain (3.5 dB) and the frequency domain (3.25 dB).

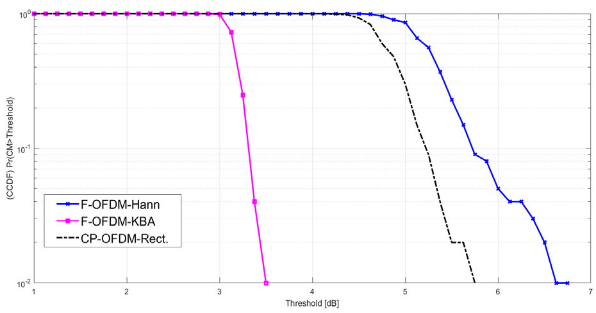

Fig. 12. Time domain evaluation of PAPR performance for the conventional 64QAM CP-OFDM with the 64QAM F-OFDM-based rectangular, Kaiser, and KBA windows.

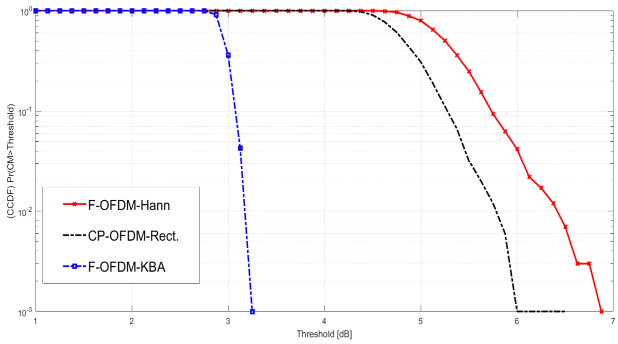

Fig. 13. Frequency domain evaluation of PAPR performance for the conventional 64QAM CP-OFDM with the 64QAM F-OFDM-based rectangular, Kaiser, and KBA windows.

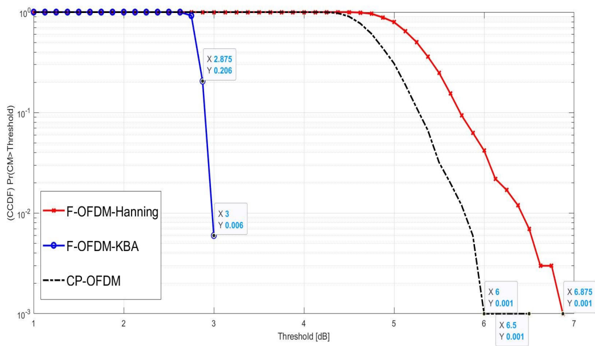

Fig. 14. Hybrid domain evaluation of PAPR performance for the conventional 64QAM CP-OFDM with the 64QAM F-OFDM-based rectangular, Kaiser, and KBA windows.

D. Computational Complexity of Waveform

The examination of the existing literature revealed that the 5G network must fulfil specific criteria, such as high processing speed, to enable low-power gadgets to function for longer durations. This study investigated the computational complexity and compared it to Orthogonal Frequency Division Multiplexing (OFDM) utilising different windowing waveforms, such as F-OFDM. The number of multiplications needed for each burst in windowing waveforms is significantly higher than those suggested by the algorithm's complexity. The study's primary findings indicate that reducing complexity significantly influences two key factors: low latency communications and low energy consumption at both the transmitter and receiver. To mitigate the presence of extraneous radiation, it is possible to employ a solitary filter at a specific terminal of the F-OFDM waveform to direct a continuous CP-OFDM signal. According to Eq. (16), the computational complexity of CP-OFDM can be estimated as $N_f(\log_2(N_f)\text{-}3) + 4$, where N_f represents the number of fast Fourier Transforms (FFTs) and Inverse Fast Fourier Transforms (IFFTs) employed in the system. Moreover, the split-radix approach employs the windowing procedure.

$$CP - OFDM_{complexity} = B \times (2 \times (N_f log_2\ N_f - 3N_f + 4) \tag{56}$$

N_f is the LTE-specified count of FFT/IFFT and B resource blocks.

$$CP - OFDM_{complexity} = B \times (2 \times (N_f log_2\ N_f - 3N_f + 4) \tag{57}$$

$$F - OFDM_{complexity} = M\times(2\times(N\ log_2\ N - 3N + 4) + 2NL + 2\times(N + NCP)\times L) \tag{58}$$

As a result, to provide a fair evaluation of all windowing options for a given waveform, it is common to represent the window length as Lw, where L denotes the window length, and w represents the order of the window (L–1). When the order of the window is increased, the system's complexity likewise increases since the length of the window must be increased as well. Regarding simulation parameters, it may be said that CP-OFDM exhibits a higher level of simplicity than F-OFDM. Significantly, the F-OFDM exhibits a higher level of simplicity than the Kaiser and the conventional F-OFDM, with due consideration given to the value of OOBE reduction. To achieve comparable OOBE performance using an alternative F-OFDM waveform, it is necessary to systematically augment the beta value through Kaiser windowing and the adjustment of the Blackman filter order. These modifications contribute to the overall complexity of the system.

E. Adjacent Channel Leakage Ratio (ACLR)

Tables III–V below illustrate the distinctions among CP-OFDM (Based), F-OFDM (standard), and F-OFDM (proposed), highlighting the enhancement in ACLR resulting from the significant improvement in out-of-band emission when employing the newly suggested filter.

TABLE III. TIME DOMAIN ACLR ANALYSES OF F-OFDM AND OFDM SYSTEMS

System	SNR	Physical Channel	ACLR (in dBm)	Main Channel Power (in dBm)	Adjacent Channel Power (in dBm)
CP-OFDM	20	AWGN	–30.20	–40.10	–70.30
F-OFDM Hanning	20	AWGN	–80	–40	–120
F-OFDM Kaiser	20	AWGN	–85.79	–31.21	–117
F-OFDM Kaier Blackman,	20	AWGN	–170.39	–30.11	–200.5

TABLE IV. FREQUENCY DOMAIN ACLR ANALYSES OF F-OFDM AND OFDM SYSTEMS

System	SNR	Physical Channel	ACLR (in dBm)	Main Channel Power (in dBm)	Adjacent Channel Power (in dBm)
CP-OFDM	20	AWGN	–30.20	–40.10	–70.30
F-OFDM Hanning	20	AWGN	–80	–40	–120
F-OFDM Kaiser	20	AWGN	–99.79	–31.21	–130
F-OFDM Kaier Blackman,	20	AWGN	–180.39	–30.11	–210.5

TABLE V. HYBRID DOMAIN ACLR ANALYSES OF F-OFDM AND OFDM SYSTEMS

System	SNR	Physical Channel	ACLR (in dBm)	Main Channel Power (in dBm)	Adjacent Channel Power (in dBm)
CP-OFDM	20	AWGN	–30.20	–40.10	–70.30
F-OFDM Hanning	20	AWGN	–80	–40	–120
F-OFDM Kaiser	20	AWGN	–87.79	–31.21	–119
F-OFDM Kaier Blackman,	20	AWGN	–220.39	–30.11	–250.5

The analysis of ACLR in the time domain for F-OFDM and OFDM systems.

F. Out-of-Band Emission (OOBE) Outcomes

To improve the performance of reducing OOBE, the windowing approach is proposed as an alternative to the widely used Hanning windowing technique for F-OFDM waveforms. In particular, where the value of K equals 1024 and M corresponds to 64QAM. The measurement of ACLR performance will be conducted following the 3GPP specification, employing the windowing technique. The performances of three distinct filters in the presence of an Additive White Gaussian Noise (AWGN) channel, with parameters K = 1024, M = 64QAM, and alpha = 3, are illustrated in Figs. 11–13. These filters include the CP-OFDM-Rectangular window, the traditional F-OFDM Hanning window, and the F-OFDM with KBA windowing. The performance of F-OFDM with KBA windowing is superior to that of CP-OFDM with rectangular windowing and F-OFDM with Hanning windowing in terms of reducing OOBE. Additionally, it is evident that the OOBE of the original Cyclic Prefix Orthogonal Frequency Division Multiplexing (CP-OFDM) signal initiates at levels of –67.55, –67.59, and –65.9 dBW/Hz in the temporal, spectral, and hybrid domains, respectively. In contrast, the conventional Filtered Orthogonal Frequency Division Multiplexing (F-OFDM) signal exhibits OOBE starting at 225.6, –225.2, and –222.7 dBW/Hz levels in the corresponding domains. Furthermore, the F-OFDM with KBA (F-OFDM-KBA) demonstrates OOBE commencing at levels of –301.7, -301.8, and –362 dBW/Hz in the three domains. The utilisation of filtering in F-OFDM effectively mitigates OOBE and eliminates the leaking of sidelobes inherent in CP-OFDM signals due to their sinusoidal characteristics.

The F-OFDM with KBA windowing outperformed both the F-OFDM with Hanning windowing and the CP-OFDM in the first, second, and third domains, with power spectral densities of –301.7, –301.8, and –362 dBW/Hz, respectively. One of the primary benefits of the F-OFDM system is its ability to mitigate OOBE in the OFDM signal. This capability enables improved frequency localisation and enhanced spectrum reuse, thereby addressing the demands of 5G applications. Furthermore, it has been demonstrated that the spectral concentration issue is most effectively addressed by employing the KBA (windowing) filter, which maximises concentration in the waveform. The alpha value can also be modified to increase the KBA's performance.

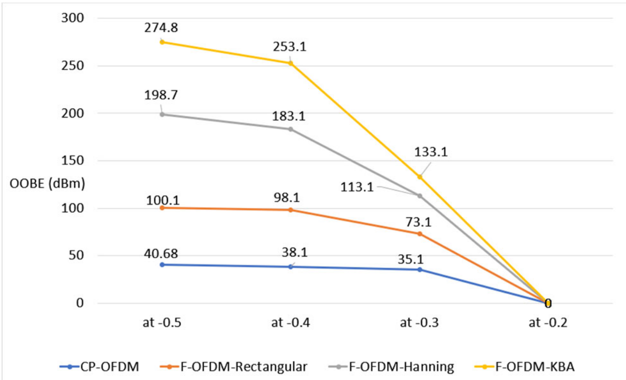

Fig. 15. Time domain evaluation of OOBE performance for the conventional 64QAM CP-OFDM with the 64QAM F-OFDM-based rectangular and KBA windows.

Fig. 15 depicts the PSD's temporal performance regarding the OOBE. The graph illustrates that the KBA OOBE exhibits an improvement of over 29%, which validates the efficacy of the new KBA filter.

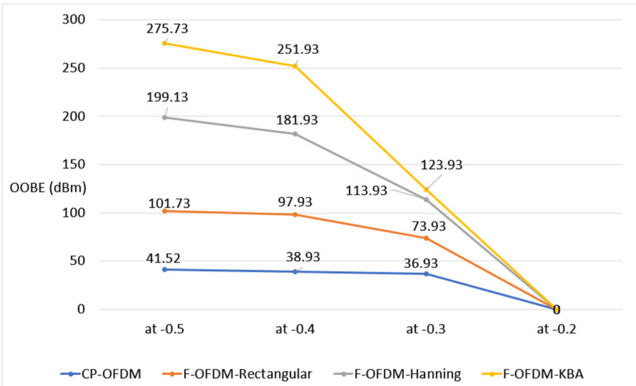

Fig. 16. Frequency domain evaluation of OOBE performance for the conventional 64QAM CP-OFDM with the 64QAM F-OFDM-based rectangular and KBA windows.

Additionally, Fig. 16 presents the PSD performance in the frequency domain, as assessed through the OOBE. The graph demonstrates that the KBA OOBE exhibits a notable improvement of over 29%, satisfying the requirements for validating the efficacy of the new filter (KBA).

Fig. 17 illustrates the PSD's performance in the hybrid domain, explicitly focusing on the OOBE. The graph demonstrates that the KBA OOBE exhibits a consistent improvement of over 41%, a commonly accepted benchmark for validating a new filter.

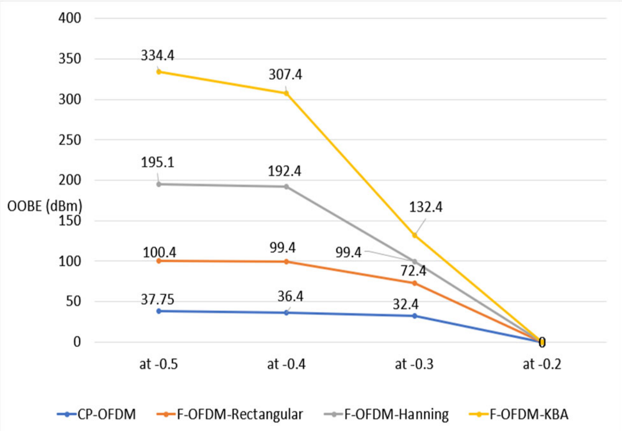

Fig. 17. Hybrid domain evaluation of OOBE performance for the conventional 64QAM CP-OFDM with the 64QAM F-OFDM-based rectangular and KBA windows.

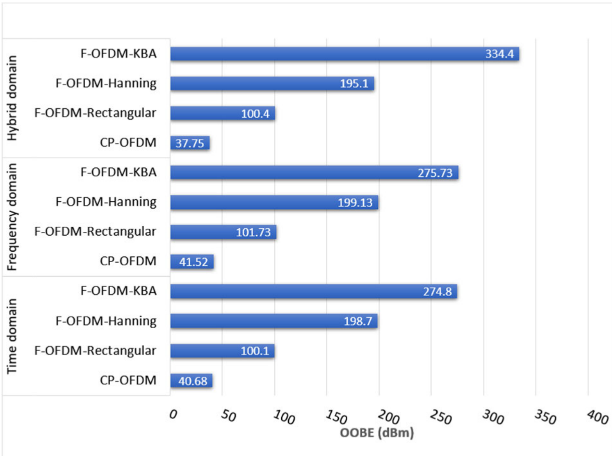

Fig. 18. Three domains evaluation of OOBE performance for the conventional 64QAM CP-OFDM with the 64QAM F-OFDM based-Rectangular and KBA windows.

Fig. 18 indicates that the KBA outperforms the other two filters in all three domains, with the most significant advantage being shown in the hybrid domain and the highest OOBE in the case of the hybrid domain.

XI. Present Outcomes and Benchmarks

The findings of this study indicate that the F-OFDM framework, as presented, presents numerous advantages when compared to existing state-of-the-art approaches. The advantages encompassed by this approach consist of the augmentation of spectral efficiency, the reduction of Inter-Carrier Interference (ICI) resulting from the improved F-OFDM signals, as well as the heightened flexibility in accommodating differences in the numerology of Frequency Range 1 (FR1) and Frequency Range 2 (FR2) employed by different services. F-OFDM performs better than CP-OFDM and classic F-OFDM while concurrently exhibiting reduced energy consumption.

Based on the analysis of KPIs for F-OFDM and CP-OFDM, employing the Hanning filter and the KBA filter with the CP-OFDM-rectangular filter, as depicted in Fig. 15, which illustrates the OOBE, PSD, BER, PAPR, and complexity, it can be concluded that the KBA filter outperforms the conventional filter in both F-OFDM and CP-OFDM systems. In the context of PSD, applying KBA in the hybrid domain demonstrates superior outcomes. Conversely, employing KBA to enhance BER in the time domain exhibits the most notable enhancement. Significant improvements are observed in both the Time and hybrid domains when the KBA filter is simultaneously implemented in PAPR. In the context of F-OFDM, utilising the KBA filter yields a complexity that surpasses that of the traditional filter in both the time and frequency domains. Using KBA leads to an improvement in the OOBE for the KPIs across all three domains. Furthermore, the OOBE demonstrates an even more significant improvement in the hybrid domain, as depicted in Fig. 16. The present study examines the PSD status among three flight conditions across three distinct domains. This study aims to investigate the status of BER across three flights operating inside three distinct domains. The current status of PAPR is being examined throughout three flights within three distinct domains. The complexity status among three flights inside three domains. The Electronic Out-of-Band Execution (e-OOBE) status concerning three flights over three domains is being reviewed. Fig. 19 depicts the status of KPIs for three flights across three domains.

Figs. 20 and 21 present a comparative analysis between the outcomes of the present study and the findings reported in the latest research papers, focusing on both the time and frequency domains. This comparison is employed to substantiate the findings. The use of the KBA filter approach yields a significantly more significant improvement than the most recent research, including factors such as the OOBE, level of competitive complexity, and other KPIs.

We will analyse the accompanying figure to assess the efficacy of the new window KBA and compare it to the conventional Hanning filter in terms of performance. The equation is integrated to calculate the area. The value of k in the Hanning filter ranges from 0 to 500, as indicated in the equation. In contrast, for the KBA filter, k ranges from 100 to 400 throughout the integration of the equation. The numerical value provided is 3.33.

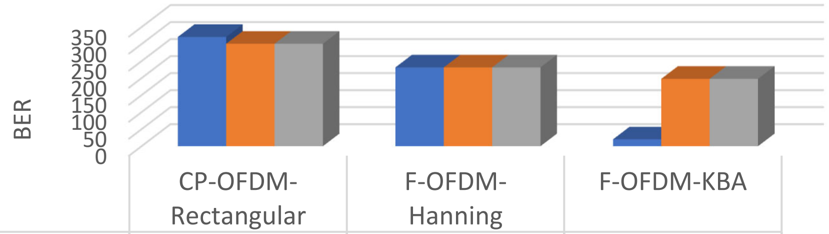

	CP-OFDM-Rectangular	F-OFDM-Hanning	F-OFDM-KBA
BER Time domine	320.9	231.5	20.06
BER Frequncy domine	300.9	231.5	198
BER Hybrid domine	300.9	231.5	198

Fig. 19. BER status between three flites within three domains.

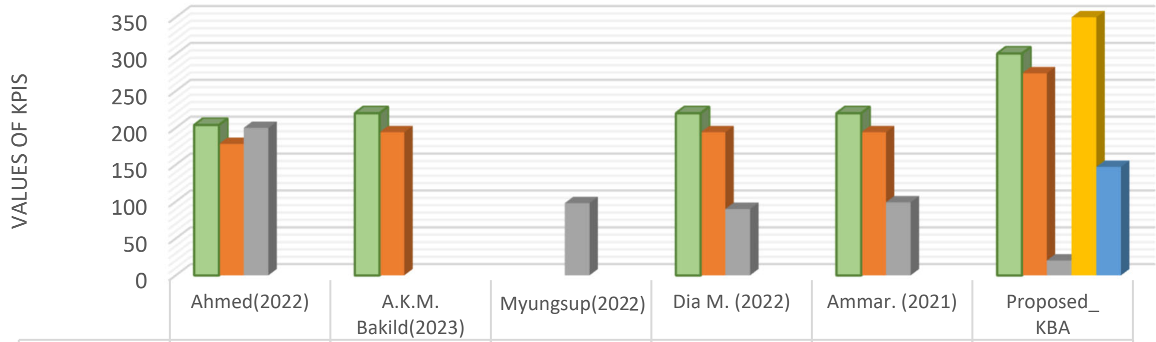

	Ahmed(2022)	A.K.M. Bakild(2023)	Myungsup(2022)	Dia M. (2022)	Ammar. (2021)	Proposed_ KBA
PSD(dB w/Hz)	204	220		220	220	301
OOBE (dBm)	178.3	194		194	194	274
BER	200		98	90	99	20.06
PAPR (dBm)						350
complexity						147

AUTHERS

Fig. 20. Comparing the latest research papers with the proposed filter in the time domain.

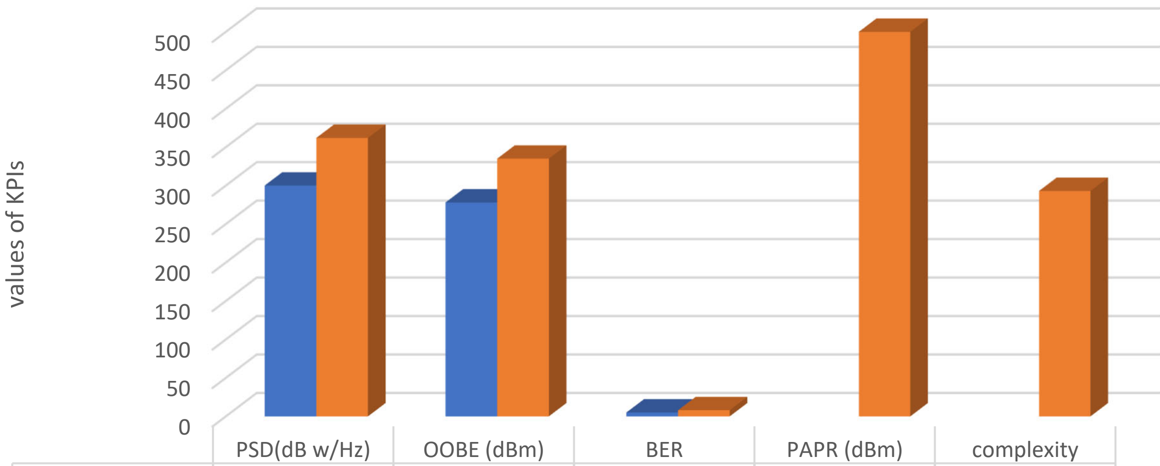

	PSD(dB w/Hz)	OOBE (dBm)	BER	PAPR (dBm)	complexity
Montadar (2020)	300	278	5		
Proposed_ KBA	362	335	8	500	293

Fig. 21. Comparing the latest research papers with the proposed filter in the frequency domain.

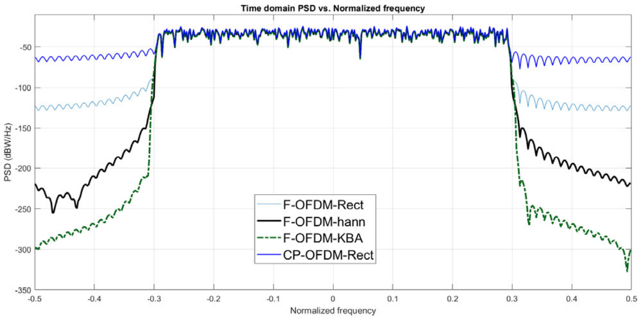

Fig. 22. Time domain 256QAM analysis for PSD of AWGN SNR = 20 dB in Hanning, KBA, and rectangular OFDM.

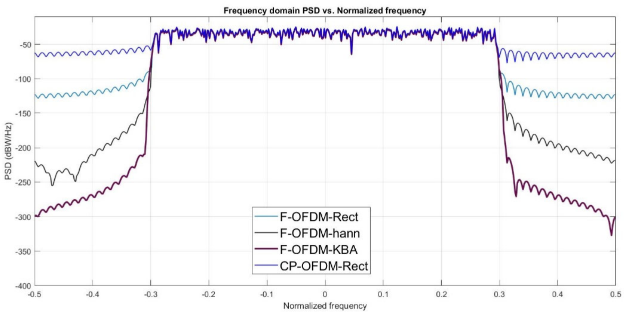

Fig. 23. Frequency domain 256QAM analysis for PSD of AWGN SNR = 20 dB in Hanning, KBA, and rectangular OFDM.

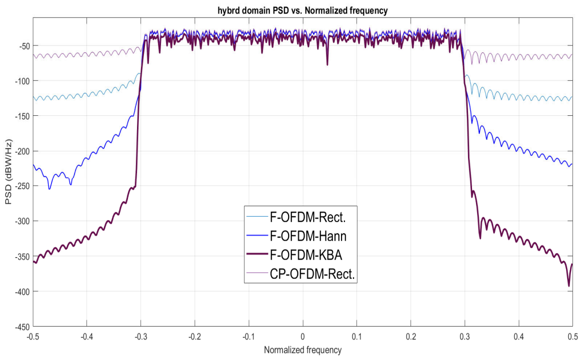

Fig. 24. Hybrid domain 256QAM analysis for PSD of AWGN SNR = 20 dB in Hanning, KBA, and Rect. OFDM.

Based on the outcomes derived from the equations mentioned above, it is evident that the amplified waveform achieved using the KBA filter surpasses that of the conventional Hanning filter. Consequently, our waveform assessment will employ the 256 QAM mapping scheme, as depicted in the accompanying figure. In this context, the Figs. 22–24, and the accompanying figure, are relevant. The numerical value is 21. In the PSD analysis across all domains, no significant differences that may be disregarded are observed, as indicated by the BER depicted in Figs. 25–27, illustrating that despite a fourfold increase in the sending, the observed difference remains quite close to that of the classic filter (Hanning). The numerical value in Fig. 28. The present study aims to examine and contrast the performance of 64QAM and 256QAM modulation schemes.

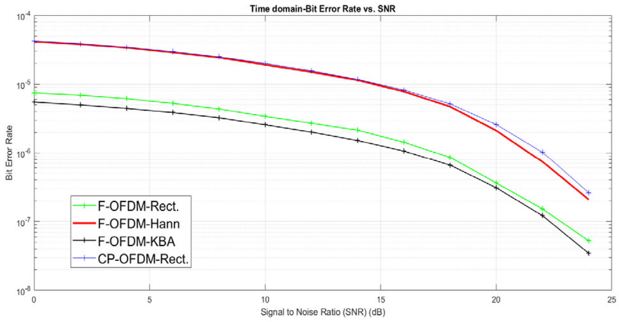

Fig. 25. Time domain evaluation of BER performance for the conventional 256QAM CP-OFDM with the 64QAM F-OFDM-based rectangular, Hanning, and KBA windows.

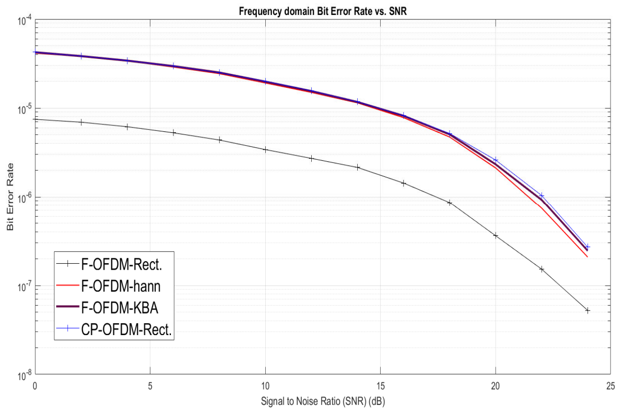

Fig. 26. Frequency domain evaluation of BER performance for the conventional 256QAM CP-OFDM with the 64QAM F-OFDM-based rectangular, Hanning, and KBA windows.

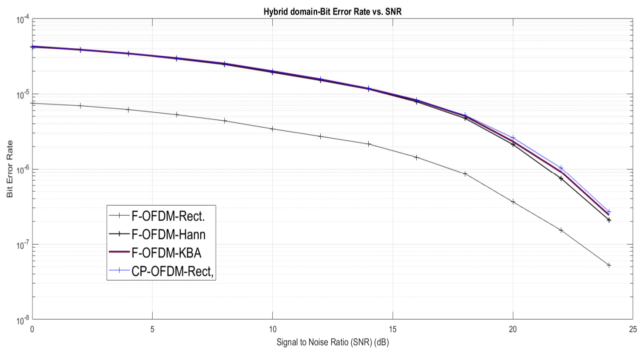

Fig. 27. Hybrid domain evaluation of BER performance for the conventional 256QAM CP-OFDM with the 64QAM F-OFDM based-Rectangular, Hanning, and KBA windows.

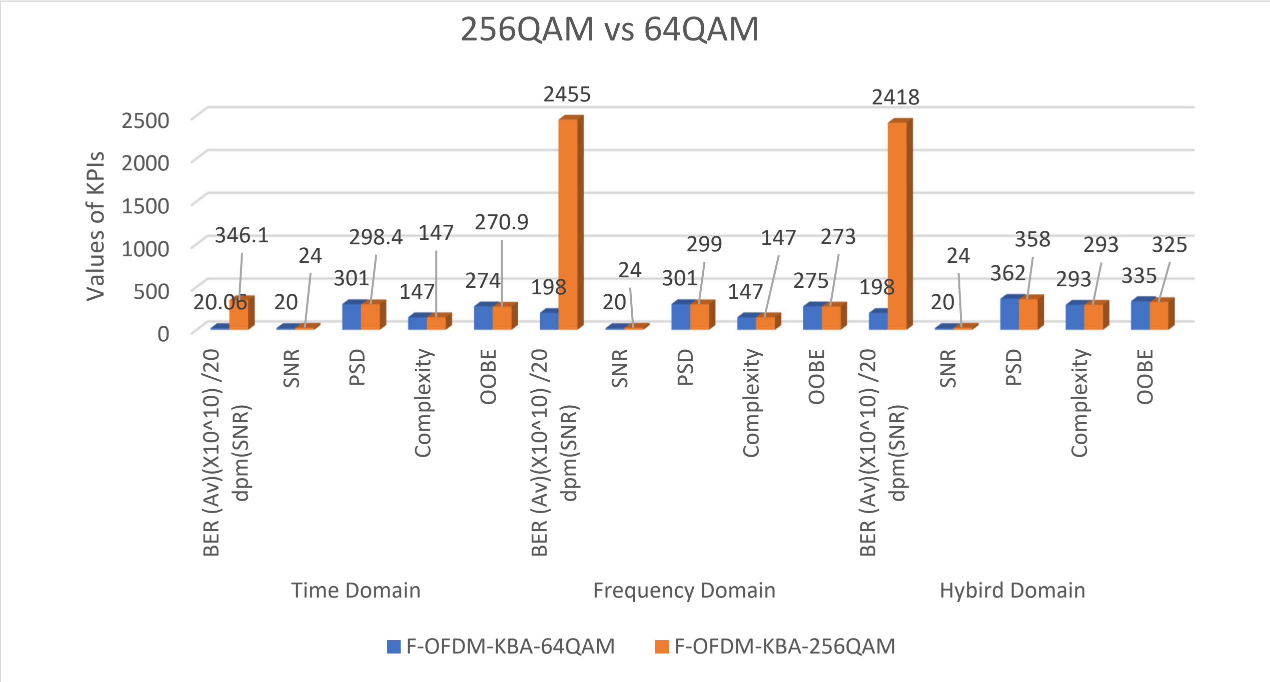

Fig. 28. Comparing KPIs in three domains (time, frequency and hybrid domains) with 256QAM.

XII. Conclusions and Future Works

This work uses windowing to build novel F-OFDM techniques to reduce OOBE while reducing computer complexity. This research created novel time-domain windowing methods. Instead of the conventional waveform, we designed KBA windowing to decrease OOBE while maintaining windowing extent and reducing processing costs. New frequency domain methods are being tested to minimise OOBE and processing complexity in 5G networks while maintaining practicality.

A hybrid domain technique combines temporal and frequency domain best practices. The purpose is to reduce out-of-band emissions.

Three methods verified this work's strategy and techniques. Simulation in MATLAB will start. The windowing methods' impacts on OOBE, computational complexity, BER, and power spectral density are tested. KBA beats Hanning and CP-OFDM-rectangular filters in OOBE, PSD, BER, PAPR, and computational complexity. KBA boosts hybrid domain PSD and time domain BER the most. PAPR KBA filters boost hybrid performance and time. KBA filters surpass F-OFDM filters in time and frequency. KBA improves the first OOBE user experience for assessing KPIs in all three areas. However, the hybrid domain OOBE improves the most. The new filter KBA must provide a 29% in-time domain increase over out-of-band emissions to succeed. Additionally, OOBE boosts frequency domain power spectral density by 29%. These metrics verify KBA filters. The KBA's hybrid domain PSD and OOBE have continuously improved by over 41%, a filter validation requirement. The KBA filter beats the others in all three categories. The hybrid domain gives it the most excellent out-of-band energy; therefore, this benefit is prominent.

The KBA window's performance was compared to the Hanning filter employing 256 QAM mapping. Despite quadrupling the standard Hanning filter's transmission, PSD stays identical across all domains. THE BER differs somewhat but is close to the typical filter. Finally, KBA, the novel filter, should use 256QAM instead of 64QAM. This research suggests that 5G and future networks use FBMC and GFDM waveforms. The transmitter's F-OFDM algorithms may be employed for receiver windowing.

Conflict of Interest

The authors declare no conflict of interest.

Author Contributions

Ammar Ahmed conducted the research; all authors analyzed the data; Ammar Ahmed done the writing; Siti Barirab, Fadlee, and Marsyata reviewed the writing; all authors had approved the final version.

References

[1] R. O. Green, "Imaging spectroscopy and the airborne visible/infrared imaging spectrometer (AVIRIS)," *Remote Sensing of Environment*, vol. 65, no. 3, 1998.

[2] A. Pekar *et al.*, "Application domain-based overview of IoT network traffic characteristics," *ACM Comput. Surv.*, pp. 1–33, 2021.

[3] J. V. D. Beek, "Orthogonal multiplexing in a subspace of frequency well-localized signals," *IEEE Communications Letters*, vol. 14, no. 10, pp. 882–884, 2010.

[4] M. Ma, X. Huang, B. Jiao, and Y. J. Guo, "Optimal orthogonal precoding for power leakage suppression in DFT-based systems," *IEEE Transactions on Communications*, vol. 59, no. 3, pp. 844–853, 2010.

[5] H. Lin, "Flexible configured OFDM for 5G air interface," *IEEE Access*, vol. 3, pp. 1861–1870, 2015.

[6] J. Du, P. Xiao, J. Wu, and Q. Chen, "Design of isotropic orthogonal transform algorithm-based multicarrier systems with blind channel estimation," *IET Communications*, vol. 6, no. 16, pp. 2695–2704, 2012.

[7] L. Wan, Z. Guo, and X. Chen, "Enabling efficient 5G NR and 4G LTE coexistence," *IEEE Wireless Communications*, vol. 26, no. 1, pp. 6–8, 2019.

[8] N. Taşpinar and Ş. Şimşir, "PAPR reduction based on partial transmit sequence technique in UFMC waveform," in *Proc. Iberian Conference on Information Systems and Technologies (CISTI)*, 2019, pp. 1–6.

[9] M. Mukherjee, R. Y. Chang, and V. Kumar, "OFDM-based overlay cognitive radios with improved spectral leakage suppression for future generation communications," *IEEE Wireless Communications and Networking Conference (WCNC)*, pp. 434–439, 2015.

[10] S. Sujatha and P. Dananjayan, "PAPR reduction techniques in of dm systems using DCT and IDCT," *Computer Science and Engineering*, 2014.

[11] J. Roostaei, Y. Z. Wager, W. Shi, T. Dittrich, C. Miller, and K. Gopalakrishnan, "IoT-based edge computing (IoTEC) for improved environmental monitoring," *Sustainable Computing: Informatics and Systems*, vol. 38, 2023.

[12] G. R. A. Juboori, A. Doufexi, and A. R. Nix, "System level 5G evaluation of GFDM waveforms in an LTE-A platform," *Wireless Communication Systems (ISWCS)*, pp. 335–340, 2016.

[13] I. S. Gaspar, L. L. Mendes, N. Michailow, and G. Fettweis, "A synchronisation technique for generalised frequency division multiplexing," *EURASIP Journal on Advances in Signal Processing*, no. 1, p. 67, 2014.

[14] P. N. Rani and C. S. Rani, "UFMC: The 5G modulation technique," in *Proc. IEEE International Conference on Computational Intelligence and Computing Research (ICCIC)*, 2016, pp. 1–3.

[15] E. Kofidis *et al.*, "Chapter 14 – MIMO-FBMC receivers," *Orthogonal Waveforms and Filter Banks for Future Communication Systems*, pp. 375-406, 2017.

[16] M. Bellanger *et al.*, "FBMC physical layer: A primer," *PHYDYAS*, vol. 25, no. 4, pp. 7–10, January 2010.

[17] M. J. Abdoli, M. Jia, and J. Ma, "Weighted circularly convolved filtering in OFDM/OQAM," *Personal Indoor and Mobile Radio Communications (PIMRC)*, pp. 657–661, 2013.

[18] T. Taheri, M. Mohamad, R. Nilsson, and J. van de Beek, "Joint spectral-spatial precoders in MIMO-OFDM transmitters," *Signal Processing*, 107538, 2020.

[19] C. An, B. Kim, and H.-G. Ryu, "WR-OFDM system and OOB spectrum comparison," in *Proc. Ninth International Conference on Ubiquitous and Future Networks (ICUFN)*, pp. 373–377, 2017.

[20] C. An, B. Kim, and H.-G. Ryu, "WF-OFDM (windowing and filtering OFDM) system for the 5G new radio waveform," in *Proc. IEEE XXIV International Conference on Electronics, Electrical Engineering and Computing (INTERCON)*, pp. 1–4, 2017.

[21] K. Hussain and R. López-Valcarce, "Optimal window design for W-OFDM," in *Proc. ICASSP 2020-2020 IEEE International Conference on Acoustics, Speech and Signal Processing (ICASSP)*, pp. 5275–5289, 2020.

[22] A. Sahin and H. Arslan, "Edge windowing for OFDM based systems," *IEEE Communications Letters*, vol. 15, no. 11, pp. 1208–1211, 2011.

[23] L. Yang and Y. Xu, "Filtered-OFDM system performance research based on Nuttall's Blackman-Harris window," in *Proc. 2017 IEEE 17th International Conference on Communication Technology (ICCT)*, 2017, pp. 687–691.

[24] R. Dayana and R. Kumar, "Sub-band filter in universal filtered multi-carrier transceiver for the cognitive radio network," *Wireless Personal Communications*, vol. 103, no. 2, pp. 1587–1602, 2018.

[25] G. Wunder, P. Jung, M. Kasparick, T. Wild, F. Schaich, Y. Chen, S. T. Brink, I. Gaspar, N. Michailow, A. Festag, L. Mendes, N. Cassiau, D. Ktenas, M. Dryjanski, S. Pietrzyk, B. Eged, P. Vago, and F. Wiedmann, "5GNOW: Non-orthogonal, asynchronous waveforms for future mobile applications," *IEEE Communications Magazine*, vol. 52, no. 2, pp. 97–105, 2014.

[26] P. Banelli, S. Buzzi, G. Colavolpe, A. Modenini, F. Rusek, and A. Ugolini, "Modulation formats and waveforms for 5G networks: Who will be the heir of OFDM?: An overview of alternative modulation schemes for improved spectral efficiency," *IEEE Signal Processing Magazine*, vol. 31, no. 6, pp. 80–93, 2014.

[27] J. Yli-Kaakinen, T. Levanen, M. Renfors, and M. Valkama, "Optimized fast convolution-based filtered-OFDM processing for 5G," in *Proc. European Conference on Networks and Communications (EuCNC)*, 2017, pp. 1–6.

[28] A. Sahin, R. Yang, M. Ghosh, and R. L. Olesen, "An improved unique word DFT-Spread OFDM scheme for 5G systems," *IEEE Globecom Workshops (GC Wkshps)*, pp. 1–6, 2015.

[29] Y. Zhao, X. Hao, Z. Liu, H. Wu, and S. Ding, "Resource block filtered-OFDM as a multi-carrier transmission scheme for 5G," *Computers and Electrical Engineering*, vol. 72, 2018.

[30] A. A. Dulaimi, X. Wang, and I. C. Lin, *Waveform Design for 5G and Beyond*, arXiv:1902.05999, 2018.

[31] A. F. Almutairi and A. Krishna, "Filtered-orthogonal wavelet division multiplexing (F-OWDM) technique for 5G and beyond communication systems," *Scientific Reports*, 4607, 2022.

[32] A. I. Zaki, A. A. Hendy, W. K. Badawi, and E. F. Badran, "Joint PAPR reduction and sidelobe suppression in NC-OFDM based cognitive radio using wavelet packet and SC techniques," *Physical Communication*, vol. 35, 100695, 2019.

[33] H. Chen and K. Chung, "A PTS technique with non-disjoint sub-block partitions in M-QAM OFDM systems," *IEEE Transactions on Broadcasting*, vol. 64, no. 1, pp. 146–152, 2018.

[34] P. Guan, D. Wu, T. Tian, J. Zhou, X. Zhang, L. Gu, A. Benjebbour, M. Iwabuchi, and Y. Kishiyama, "5G field trials: OFDM-based waveforms and mixed numerologies," *IEEE Journal on Selected Areas in Communications*, vol. 35, no. 6, pp. 1234–1243, 2017.

[35] M. Ahmed, N. Shah, F. Ghawbar, Y. Jawhar, and A. Almohammedi, "Filtered-OFDM with channel coding based on T-distribution noise for underwater acoustic communication," *Journal of Ambient Intelligence and Humanized Computing*, vo. 13, pp. 3379–3392 2020.

[36] F. Conceição, M. Gomes, V. Silva, and R. Dinis, "An OFDM-based waveform with high spectral efficiency," *IEEE Communications Letters*, vo. 24, no. 11, 2020.

[37] M. Ishibashi, M. Umehira, W. Xiaoyan, and S. Takeda, "FFT-based frequency domain filter design for multichannel overlap-windowed-DFTs-OFDM signals," in *Proc. IEEE 93rd Vehicular Technology Conference (VTC2021-Spring)*, 2021, pp. 1–5.

[38] T. Taheri, M. Mohamad, R. Nilsson, and J. van de Beek, "Joint spectral-spatial precoders in MIMO-OFDM transmitters," *Signal Processing*, 107538, 2020.

[39] 3GPP, "5G new radio: Introduction to the white paper," *ComSoc*, 2018.

[40] E. Bala *et al*., "Shaping spectral leakage: A novel low-complexity transceiver architecture for cognitive radio," *IEEE Vehicular Technology Magaz*ine, vol. 8, no. 3, 2013.

[41] 3GPP TS 36.104, Technical specification group radio access network; Evolved Universal Terrestrial Radio Access (E-UTRA). Base Station (BS) radio transmission and reception, v8.2.0, May 2008.

[42] R. S. Yarrabothu, N. Kanchukommula, and U. R. Nelakuditi, "Design and analysis of Universal-Filtered Multi-carrier (UFMC) waveform for 5G cellular communications using kaiser filter," *Soft Computing and Signal Processing*, pp. 721–730, 2019.

[43] M. Ishibashi, M. Umehira, W. Xiaoyan, and S. Takeda, "FFT-based frequency domain filter design for multichannel overlap-windowed-DFTs-OFDM signals," in *Proc. IEEE 93rd Vehicular Technology Conference (VTC2021-Spring)*, 2021, pp. 1–5.

[44] X. Cheng, Y. He, B. Ge, and C. He, "A filtered OFDM using FIR filter based on window function method," in *Proc. IEEE 83rd Vehicular Technology Conference (VTC Spring)*, Nanjing, China, pp. 1–5, 2016.

[45] G. Barb and M. Otesteanu, "4G/5G: A comparative study and overview on what to expect from 5G," in *Proc. 2020 43rd International Conference on Telecommunications and Signal Processing (TSP)*, 2020, pp. 37–40.

[46] K. Hussain and R. L. Valcarce, "Optimal window design for W-OFDM," in *Proc. ICASSP – IEEE International Conference on Acoustics, Speech and Signal Processing (ICASSP)*, 2020, pp. 5275–5289.

[47] R. S. Yarrabothu and U. R. Nelakuditi, "Optimization of out-of-band emission using kaiser-vessel filter for UFMC in 5G cellular

communications," *China Communications*, vol. 16, no. 8, pp. 15−23, 2019.

[48] V. Kumar, S. Bangar, S. N. Kumar, and S. Jit, "Design of effective window function for FIR filters," in *Proc. International Conference on Advances in Engineering and Technology Research (ICAETR-2014)*, 2014, pp. 1−5.

[49] H. Rakshit and M. A. Ullah, "An adjustable novel Window function with its application to FIR filter design," in *Proc—international Conference on Computer and Information Engineering (ICCIE)*, 2015, pp. 36–41.

[50] D. Kalaiyarasi and T. K. Reddy, "A hybrid window function to design finite impulse response low pass filter with an improved frequency response," in *Proc. International Conference on Energy, Communication, Data Analytics and Soft Computing (ICECDS)*, 2017, pp. 138−143.

[51] A. Hammoodi, L. Audah, L. Al-Jobouri, M. A. Mohammed, and M. S. Aljumaily, "New 5G kaiser-based windowing to reduce out-of-band emission," *Computers, Materials and Continua*, vol. 71, no. 2, 2022.